

Supersonic dislocations observed in a plasma crystal

V. Nosenko, S. Zhdanov, G. Morfill

Max-Planck-Institut für extraterrestrische Physik, D-85741 Garching, Germany

(Dated: October 22, 2018)

Abstract

Experimental results on the dislocation dynamics in a two-dimensional plasma crystal are presented. Edge dislocations were created in pairs in lattice locations where the internal shear stress exceeded a threshold and then moved apart in the glide plane at a speed higher than the sound speed of shear waves, C_T . The experimental system, a plasma crystal, allowed observation of this process at an atomistic (kinetic) level. The early stage of this process is identified as a stacking fault. At a later stage, supersonically moving dislocations generated shear-wave Mach cones.

PACS numbers: 52.27.Lw, 52.27.Gr, 61.72.Ff, 82.70.Dd

Dislocations are ubiquitous in solids [1]. They are essential to understanding such properties as plasticity, yield stress, susceptibility to fatigue, fracture, and dislocation-mediated melting of 2D solids. Dislocation generation and motion is therefore of interest in materials science [2], the study of earthquakes [3], snow avalanches [4], colloidal crystals [5], 2D foams [6], and various types of shear cracks [7, 8].

The theory of dislocations uses several approaches. In elastic theory, a dislocation’s core is treated as a singularity in an otherwise continuous elastic material. Linear elastic theory predicts that a gliding edge dislocation cannot overcome the sound speed of shear waves C_T , because the energy radiated by a moving dislocation becomes infinite at this speed. However, a gliding edge dislocation can move at a particular speed of $\sqrt{2}C_T$ [9]; in this case, it does not emit any radiation at all and therefore its motion is frictionless. A more detailed theory of dislocations should take into account the discrete “atomistic” structure of matter. In Ref. [9], this was taken into account in the dislocation’s glide plane, outside, the material was considered to be an elastic continuum. Then, the limiting speed for dislocations is the Rayleigh wave speed C_R ; usually, $C_R \lesssim C_T$.

Gliding edge dislocations moving at the speed of $1.3C_T$ to $1.6C_T$ were observed in atomistic computer simulations [10]. Dislocations were created with a speed exceeding C_T at a strong stress concentration. High shear stress was required to sustain their motion. Dislocations always radiated strongly, even when they traveled at exactly $\sqrt{2}C_T$. This was attributed to nonlinear effects in the dislocation core. Shear cracks propagating faster than C_T were observed in Ref. [8]. However, to the best of our knowledge, experimental evidence that dislocations can move faster than C_T is lacking.

In regular solids dislocation dynamics is almost impossible to study experimentally at an atomistic level [11] because of the small distances between the atoms (or molecules), high characteristic frequencies, and the lack of experimental techniques of visualizing the motion of individual atoms or molecules.

The most suitable model systems to experimentally study dislocations at an atomistic level are plasma crystals [12]. These are suspensions of highly charged micron-sized particles in a plasma, which can be strongly coupled [13]. Then their mutual interaction causes them to self-organize in structures that can have crystalline or liquid order. The interparticle distance can be of the order of $100 \mu\text{m}$ to 1 mm , characteristic frequencies are of the order of $10 - 100 \text{ s}^{-1}$, and the speed of sound is of the order of 10 mm/s . In addition, the absence

of a substantial background medium (as in the case of colloids) allows studies of the full dynamics without overdamping. These unique characteristics, plus the direct imaging, make it possible to study the complex dynamics of crystalline defects [14], including dislocation nucleation and motion [12, 15], all at an atomistic level.

Our experimental setup was a modified GEC chamber as in Ref. [16], using similar experimental parameters. Argon plasma was produced using a capacitively-coupled rf discharge. We used 42 W of rf power at 13.56 MHz, with an amplitude of 158 V peak-to-peak. The self-bias voltage was -96 V. To ensure that the system was not overdamped, a relatively low pressure of 3 mTorr was used. The neutral-gas damping rate is then accurately modeled [17] by the Epstein expression $\nu = \delta N_g m_g \bar{v}_g (\rho_p r_p)^{-1}$, where N_g , m_g , and \bar{v}_g are the number density, mass, and mean thermal speed of gas atoms and ρ_p , r_p are the mass density and radius of the particles, respectively. With leading coefficient $\delta = 1.26$ [17], this gave $\nu = 0.52 \text{ s}^{-1}$.

A monolayer of highly charged microspheres was levitated against gravity in the sheath above the lower rf electrode. The particles had a diameter of $8.09 \pm 0.18 \text{ }\mu\text{m}$ [17] and a mass $m = 4.2 \times 10^{-13} \text{ kg}$. The monolayer included ≈ 4500 particles, had a diameter of $\approx 60 \text{ mm}$, and rotated slowly in the horizontal plane.

The interparticle potential for particles arranged in a single plane, like ours, is well approximated [18] by the Yukawa potential: $U(r) = Q(4\pi\epsilon_0 r)^{-1} \exp(-r/\lambda_D)$, where Q is the particle charge and λ_D is the screening length. The monolayer is characterized by a screening parameter $\kappa = b/\lambda_D$, where b is the interparticle spacing. In our experiment, $b = 0.69 \text{ mm}$. We used the pulse technique of Ref. [19], making use of a theoretical wave dispersion relation [20, 21], to measure $\kappa = 1.58 \pm 0.22$ and $Q = -15\,000 \pm 1400e$. The average sound speeds in the central part of our plasma crystal were measured to be $C_L = 24.0 \pm 1.7 \text{ mm/s}$ and $C_T = 6.3 \pm 0.6 \text{ mm/s}$, for compressional and shear waves respectively. (Based on these measurements, the Rayleigh wave speed is $C_R \approx 6.0 \text{ mm/s} = 0.95C_T$, formally using the approach of Ref. [9]).

The particles were imaged through the top window by a digital camera. We recorded movies of 1024 frames at 29.88 frames per second. The $61.1 \times 45.8 \text{ mm}^2$ field of view included ≈ 4200 particles. The particle coordinates x, y and velocities v_x, v_y were then calculated with subpixel resolution for each particle in each frame.

At our experimental conditions, the particle suspension self-organized in an ordered tri-

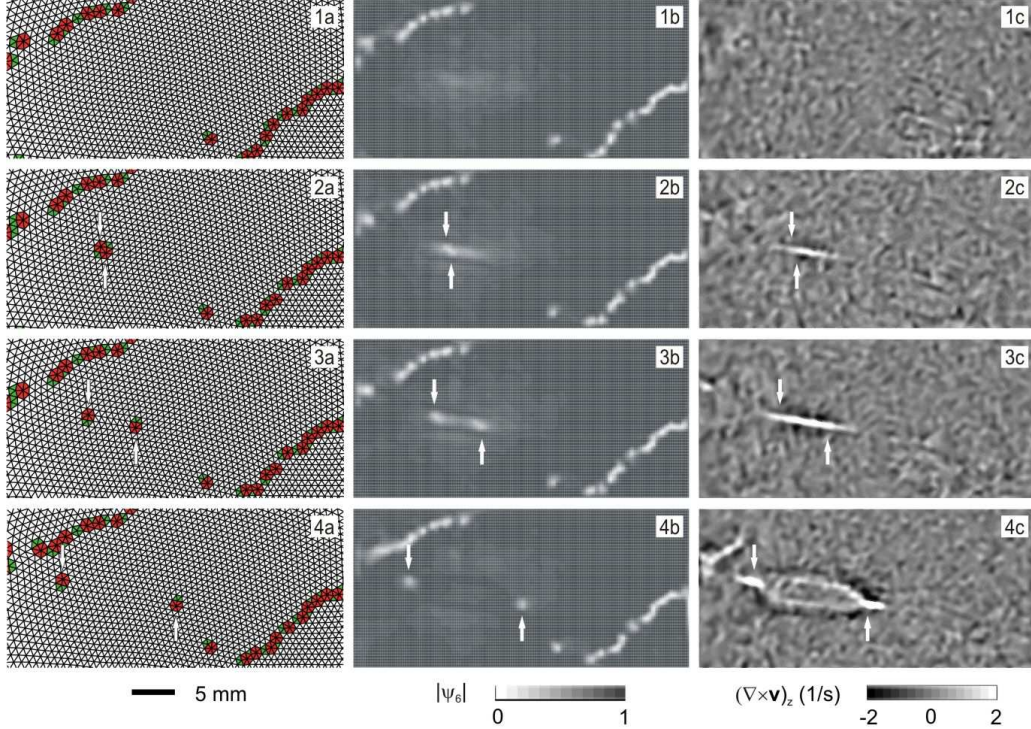


Fig. 1

FIG. 1: (Color online) Dislocation nucleation and motion in a 2D crystalline lattice. Maps of (a) triangulation of the particle positions, (b) bond-orientational function $|\psi_6|$, and (c) vorticity $(\nabla \times \mathbf{v})_z$, where \mathbf{v} is the particle velocity, are shown for four different instants of time: (1) 0.335 s, (2) 0.569 s, (3) 0.669 s, and (4) 1.004 s. A pair of dislocations, indicated by arrows, was created shortly before (2).

angular lattice with hexagonal symmetry. This lattice always contained defects, as revealed by Delaunay triangulation, Fig. 1(a). A defect is defined as a lattice site where a particle has a number of nearest neighbors other than six. Defects are highlighted in Fig. 1(a). Most of them form linear chains that constitute domain walls in our 2D crystal. Two nearly parallel domain walls are seen in Fig. 1(a).

An edge dislocation in our 2D crystal consists of an isolated pair of 5- and 7-fold defects. During the course of experiment, dislocations in the lattice are continuously generated due to the shear introduced by the slow rotation. They move around and annihilate with each other or with domain walls. Some of them may remain stationary for some time. In this Letter, we show that edge dislocations are created in pairs in lattice locations where the internal shear stress exceeds a threshold and then move apart supersonically.

To study dislocation nucleation, we evaluate the shear strain in the lattice from the bond-orientational function $|\psi_6|$ [22], shown in Fig. 1(b). For every site in the lattice, $\psi_6 = \frac{1}{n} \sum_{j=1}^n \exp(6i\Theta_j)$, where Θ_j are bond orientation angles for n nearest neighbors. In the limit of weak *simple shear*, the following relation can be used: $|\psi_6| = 1 - 9\gamma^2$, where γ is the shear strain. For weak *pure shear*, $|\psi_6| = 1 - 2.25e^2$, where e is elongation, which is the measure of pure shear deformation. We derived these relations assuming small deformations of an elementary hexagonal cell. Note that $|\psi_6|$ is insensitive to uniform compressions, rotations, and translations, i.e., the deformations that do not involve any variation of bond orientations inside an elementary cell.

To study dislocation dynamics, we use the maps of vorticity $(\nabla \times \mathbf{v})_z$, Fig. 1(c), where \mathbf{v} is the particle velocity (z denotes the out-of-plane component of vorticity). These reveal shear motion [19, 23] and are therefore suitable for visualizing moving dislocations.

The shear strain in the lattice had a non-uniform distribution, as follows from Fig. 1(b). The shear strain was higher (or $|\psi_6|$ lower) in two kinds of locations. First, it was high in domain walls - the two nearly-parallel bright stripes in Fig. 1(b) (or equivalently the chains of 5- and 7-fold defects in Fig. 1(a)). Second, a “diffuse” concentration of shear strain appeared between the domain walls. We attribute this diffuse strain concentration to the differential rotation and shear in the lattice, with two “rigid” domain walls imbedded in it.

The diffuse shear strain increased with time. When it locally exceeded a certain threshold, a pair of edge dislocations was created in that location, Fig. 1(2). These dislocations appear as bright spots in Fig. 1(2b) or as pairs of 5- and 7-fold defects in Fig. 1(2a), all indicated by arrows. Once a pair of dislocations was created, they moved rapidly apart, Figs. 1(3),1(4).

During the course of our 5.7 min experiment we observed about 30 events of dislocation nucleation similar to that shown in Fig. 1. Two more typical examples are shown in Fig. 2. The “black” and “white” dislocations have opposite directions of the particle rearrangement in their cores.

We examine the dislocation nucleation and dynamics in more detail. The time evolution of the shear strain in the lattice location where a pair of dislocations is generated has several stages, as shown in Fig. 3(a). First, the shear strain builds up gradually in a certain location ($|\psi_6|$ decreases). Second, when the shear strain in this location exceeds a certain threshold, a pair of dislocations is born. Third, the shear stress is rapidly relieved when the dislocations separate, and gradually drops to the background value. This cycle then starts over again,

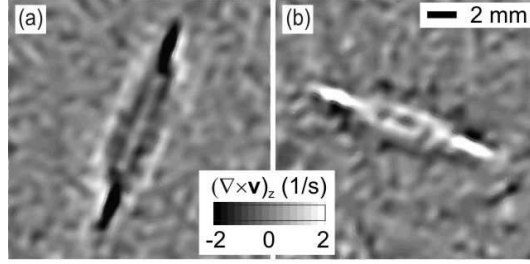


Fig. 2

FIG. 2: More examples of dislocation nucleation similar to that in Fig. 1(4c). In (a) “black” and (b) “white” dislocation cores, particles rearrange in the clockwise and counterclockwise directions, respectively.

perhaps in a different location.

When a pair of dislocations is created, their Burgers vectors are oppositely directed and equal in magnitude, within the experimental errors and inhomogeneity of the lattice. Therefore, the total Burgers vector is conserved in this process. (The Burgers vector represents the magnitude and direction of the crystalline lattice distortion by a dislocation.)

When the two dislocations separate, they leave a stacking fault between them. It appears as a narrow (one lattice constant) band where the lattice structure is distorted from triangular to nearly square, Fig. 1(3a). This stacking fault has a dynamic nature; the lattice is restored to its original state by rapid particle rearrangement that is seen as shear motion in Fig. 1(3c). A similar shear motion occurs even ahead of the right-hand-side dislocation in Fig. 1(2c).

Next, we analyze the speed of the dislocations as they move apart. Fig. 3(b) shows a grey-scale space-time plot of vorticity $(\nabla \times \mathbf{v})_z$ measured along the dislocations’ glide plane. Superimposed are the positions of dislocation cores. Note that the dislocation motion is not smooth; rather, it is of a stick-and-slip type. The average dislocation speeds are higher than C_T ; however, they decrease as dislocations move. (The slope corresponding to C_T is shown by a dashed line in Fig. 3(b)). For comparison, the linear shear disturbance in the upper part of Fig. 3(b) (seen as a faint black feature) travels at a speed $\approx C_T$. The average speeds of dislocations A and B are respectively $U_A = 9.5$ mm/s and $U_B = 13$ mm/s. We attribute this difference to the radial variation of the local number density of our crystal. It diminished from 2.4 mm $^{-2}$ in the crystal center (B moved in this direction) to ≈ 1.6 mm $^{-2}$

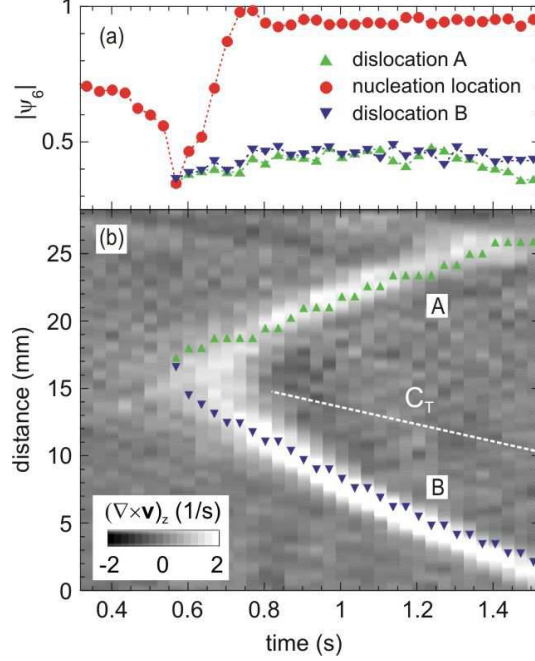


Fig. 3

FIG. 3: (Color online) Pair of dislocations is generated and moves apart. (a) Time evolution of the bond-orientational function $|\psi_6|$. We use $|\psi_6|$ to evaluate the shear strain, which is higher when $|\psi_6|$ is lower; for details, see the text. (b) The grey-scale space-time plot shows vorticity $(\nabla \times \mathbf{v})_z$ measured along the dislocations' glide plane. Superimposed are the positions of dislocation cores calculated as average positions of the respective 5- and 7-fold lattice defects. Dislocations A and B are respectively LHS and RHS in Fig. 1.

at its periphery where we still observed dislocations (A moved here).

Dislocations that move supersonically create a distinct signature, i.e., a shear-wave Mach cone, shown in Fig. 4(a). The structure is similar to that observed in Refs. [10, 19, 23]. A Mach cone is a V-shaped wake created by a moving supersonic disturbance. Mach cones obey the Mach cone angle relation $\sin \mu = C/U$, where μ is the cone's opening angle, C is the speed of sound, and U is the speed of the supersonic disturbance. From their Mach cone angles, we derive the relative speeds of dislocations A and B in Fig. 3, $U_A = 1.7C_T$ and $U_B = 1.9C_T$. Since we measured $U_A = 9.5$ mm/s and $U_B = 13$ mm/s by defect tracking, we can estimate the *local* sound speeds at the locations of A and B as $C_{T,A} = 5.5$ mm/s and $C_{T,B} = 6.7$ mm/s, respectively. Hence, C_T was higher in the crystal center and somewhat declined toward its periphery due to the corresponding decline in the crystal's number density. A weak

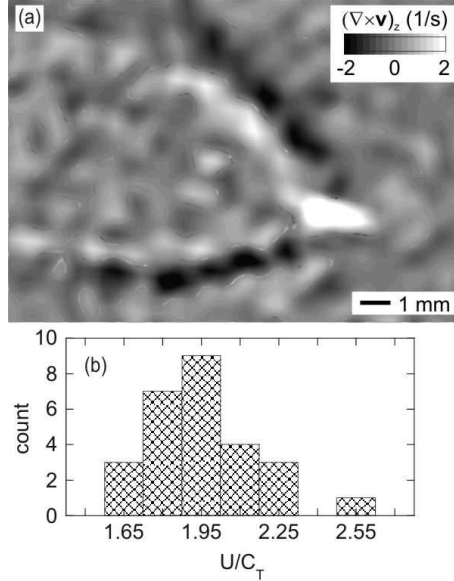


Fig. 4

FIG. 4: (a) Shear-wave Mach cone generated by a supersonically moving dislocation B from Fig. 3, at $t = 1.406$ s. (b) Distribution of supersonic dislocation speeds U .

dependence of C_T on number density (or interparticle spacing) was discussed in Ref. [20]. The Mach cones created by a dislocation pair were connected by two parallel fronts of shear waves, Fig. 1(4c). This wave front configuration evolved from the particle rearrangement in the stacking fault, Fig. 1(3c). The Mach cones were composed of shear waves and not of compressional waves, because they were excited by dislocations moving faster than C_T , but slower than C_L . Note that we did not use any external exciter as in Refs. [19, 23, 24]; also there were no particles above or beneath the monolayer as in Ref. [25].

Finally, we calculated the distribution of dislocation speeds, Fig. 4(b), using the Mach cone angle relation and measuring the opening angles of well-developed Mach cones in maps like that in Fig. 4(a). From this distribution, we conclude that the average speed of supersonic dislocations in our experiment was $(1.95 \pm 0.2)C_T$, where C_T is the sound speed of shear waves.

We thank J. Goree and T. Sheridan for their help in conducting the experiment.

[1] F. Frank, *Advances in Physics* **1**, 91 (1952).

- [2] C. Kittel, *Introduction to solid state physics*, 2nd ed. (John Wiley & Sons, New York, 1961).
- [3] R.J. Archuleta, Bull. Seismol. Soc. Am. **72**, 1927 (1982).
- [4] H.O.K. Kirchner, G. Michot, and J. Schweizer, Phys. Rev. E **66**, 027103 (2002).
- [5] P. Schall, J. Cohen, D.A. Weitz, and F. Spaepen, Science **305**, 1944 (2004); H.R. Kolar, J.C.H. Spence, and H. Alexander, Phys. Rev. Lett. **77**, 4031 (1996).
- [6] A. Abd el Kader and J.C. Earnshaw, Phys. Rev. Lett. **82**, 2610 (1999).
- [7] F.F. Abraham and H. Gao, Phys. Rev. Lett. **84**, 3113 (2000).
- [8] A.J. Rosakis, O. Samudrala, and D. Coker, Science **284**, 1337 (1999).
- [9] J.D. Eshelby, Proc. R. Soc. London A **62**, 307 (1949).
- [10] P. Gumbsch and H. Gao, Science **283**, 965 (1999).
- [11] M. Murayama, J.M. Howe, H. Hidaka, and S. Takaki, Science **295**, 2433 (2002).
- [12] Chi-Hui Chiang and Lin I, Phys. Rev. Lett. **77**, 647 (1996).
- [13] H. Thomas *et al.*, Phys. Rev. Lett. **73**, 652 (1994); J.H. Chu and Lin I, Phys. Rev. Lett. **72**, 4009 (1994); H.M. Thomas and G.E. Morfill, Nature (London) **379**, 806 (1996).
- [14] Wei-Yen Woon and Lin I, Phys. Rev. Lett. **92**, 065003 (2004); Chia-Ling Chan, Wei-Yen Woon, and Lin I, Phys. Rev. Lett. **93**, 220602 (2004).
- [15] C. Reichhardt and C.J.O. Reichhardt, Phys. Rev. Lett. **90**, 095504 (2003).
- [16] V. Nosenko, J. Goree, and A. Piel, Phys. Plasmas **13**, 032106 (2006).
- [17] B. Liu, J. Goree, and V. Nosenko, Phys. Plasmas **10**, 9 (2003).
- [18] U. Konopka, G.E. Morfill, and L. Ratke, Phys. Rev. Lett. **84**, 891 (2000).
- [19] V. Nosenko, J. Goree, Z.W. Ma, and A. Piel, Phys. Rev. Lett. **88**, 135001 (2002).
- [20] X. Wang, A. Bhattacharjee, and S. Hu, Phys. Rev. Lett. **86**, 2569 (2001).
- [21] S. Zhdanov, S. Nunomura, D. Samsonov, and G. Morfill, Phys. Rev. E **68**, 035401 (2003).
- [22] D.G. Grier and C.A. Murray, J. Chem. Phys. **100**, 9088 (1994); C.A. Knapek, D. Samsonov, S. Zhdanov, U. Konopka, and G.E. Morfill, Phys. Rev. Lett. **98**, 015004 (2007).
- [23] V. Nosenko, J. Goree, Z.W. Ma, D.H.E. Dubin, and A. Piel, Phys. Rev. E **68**, 056409 (2003).
- [24] A. Melzer, S. Nunomura, D. Samsonov, Z.W. Ma, and J. Goree, Phys. Rev. E **62**, 4162 (2000).
- [25] D. Samsonov *et al.*, Phys. Rev. Lett. **83**, 3649 (1999).